Analysis of fringing capacitance effect on the performance of micro-electromechanical-system-based micromachined ultrasonic air transducer

Reshmi Maity[1] ✉, *Niladri P. Maity*[1], *Koushik Guha*[2], *Srimanta Baishya*[2]

[1]*Department of Electronic and Communication Engineering, Mizoram University (A Central University), Aizawl 796 004, India*
[2]*Department of Electronic and Communication Engineering, National Institute of Technology, Silchar 788 010, India*
✉ *E-mail: reshmidas_2009@rediffmail.com*

Published in Micro & Nano Letters; Received on 15th September 2017; Revised on 19th February 2018; Accepted on 12th March 2018

The work analyses the significance of fringing capacitance in modelling effectively the amplitude of the ultrasonic waves generated by silicon nitride membrane-based micromachined ultrasonic transducer (MUT). The amplitude of the ultrasonic waves is proportional to the displacement of the biased membrane under the influence of a sinusoidal signal. Fringing capacitance is significant as for operating the transducer in the medical imaging regime of frequency range 1–10 MHz, the dimension of the electrodes of the MUT capacitor becomes comparable with the separation between them. The device is modelled first without the fringing effect and then Palmer, Landau's and Younes Ataiiyan's approaches are considered for evaluating the fringing capacitance. The device is finite element method analysed by PZFLEX 3D simulator. The membrane displacement is evaluated with variation in device structural parameters of membrane radius and thickness, electrode separation and bias voltage for an extensive range of values. Fractional percentage error of the above analytical approaches is evaluated with respect to the PZFLEX which are regarded as closest to reality. Substantial decrease in the error is observed on modelling the device with the effect of the fringing capacitance.

1. Introduction: Micromachined ultrasonic transducers (MUTs) are members of the micro-electromechanical-systems (MEMSs) family. For the last two decades they are studied effectively as medical imaging equipment [1–3]. Integrated circuit (IC) batch processing techniques fabricate MEMS devices, making them cost-effective and portable. The physical dimensions of these transducers are below 1 μm on the lower end of the dimensional spectrum. These devices have the ability to sense, control and actuate on the microscale, and generate effects on macroscale. The MUT is able to change the electrical signal into mechanical waves, that is, transmitting ultrasound, and vice versa to change mechanical pressure (reflected ultrasound waves, 'echos'), into electrical signals. Ultrasound is a non-ionising radiation, and hence is well accepted for diagnostic use even in obstetrical applications. All these characteristics have made ultrasound a widely used imaging modality in medicine. Ultrasound is particularly useful in imaging cardiac structures, the vascular system, the foetus and uterus, abdominal organs such as the liver, kidneys and gall bladder and the eye. A major challenge in future ultrasound imaging that feature large area two-dimensional (2D) transducer arrays for novel applications such as breast cancer screening is the most significant role of micromachined transducers as compared with piezoelectric counterparts [4].

Electrostatic actuation is the most prevailing method of driving MEMS-based ultrasonic devices. It is well-matched with microfabrication technology and provides power density. The structure resembles a capacitive element and they are well known as capacitive MUT (CMUT) devices. A typical CMUT element consists of a silicon nitride (Si_3N_4) membrane of thickness 750 nm and diameter 50 μm forming one of the electrodes over very small gaps (0.1–0.5 μm). The upper surface of the silicon base is metallised to form the lower electrode. Many Letters have been published to enhance the sensitivity of CMUTs [5, 6]. To facilitate the design and analysis of electrostatic actuators, explicit formulae for computing the capacitance as a function of the geometrical parameters are required. In electrostatic actuators used for medical imaging that are fabricated by present micromachining processes, the distance between the electrodes is not negligible relative to the lateral dimensions of the deformable capacitor. Therefore, fringing fields are considerable and must be accounted for when modelling the electrostatic forces. A voltage difference applied between these electrodes results in an electric field between them. The electric field does not end up abruptly at the edges of them but extends some distance away; this is known as a fringing field. There is some more electric field outside the electrodes because of the fringe fields that curves from one to the other. This causes the capacitance of the structure to be larger than what we calculate using the ideal formula. To accurately predict the capacitance of a capacitor, the fringing field must be modelled with the appropriate boundary conditions. The fringe effect is where lines of flux leap from one electrode to the next as seen in Fig. 1. The darkened thick lines represent the electrodes of CMUT: one of Si_3N_4 and the other of aluminium. The effect is greater with higher voltages and the lower distance between the electrodes and basically lead up to arcing, where current literally leaps from one conductor to the other. The fringing field comes into effect when the gap size of the electrodes is as good as their geometrical extent. Clearly, the fringing field increases the capacitance and the electrostatic force.

The fringing field effects on the capacitance of a circular parallel-plate capacitor has been of historical interest and more recently has become a fashionable topic because of the applications to the microstrip circuit and antenna elements [7]. Vitaly and David [8] have worked on the fringing field effect in electrostatic actuators. Hosseini *et al.* presented a new model in which the effect of fringing field is represented by a time-varying serial capacitor. This capacitor is applied to the control of parallel-plate electrostatic microactuators [9]. A more recent approach is the empirical formulae derived based on the experiments of ultrasonic waves [10]. Some recent works on the application of these capacitance models are also seen, where modified capacitance model of radio-frequency (RF) MEMS shunt switching incorporating fringing field effects of the perforated beam is derived [11]. Square diaphragm CMUT for fringing field effect has also been investigated [12]. In this work, we concentrate on the fringing field effect of circular membrane CMUT as they are most widely used for medical imaging purposes. To evaluate the effect, the displacement of the membrane at the centre of the device is investigated. The membrane displacement determines the amplitude of the ultrasonic waves

doi: 10.1049/mnl.2017.0688

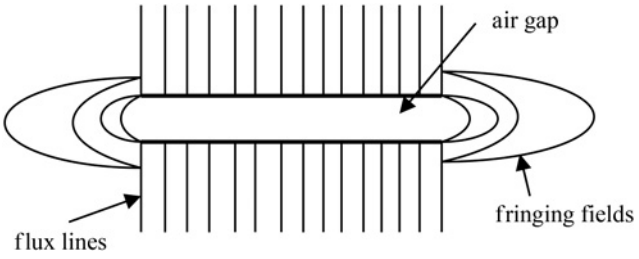

Fig. 1 *Fringing effect*

generated from the biased CMUT in the transmitter mode, which determines the efficiency of the transducer. To get the maximum efficiency from the transducer, a good design is very important. Accurately modelled transducer assists to optimise the device parameters before fabrication. The variations of the displacement for the device structural and physical parameters are analysed for a wide range of values. The displacement is first evaluated without fringing field effect and later three most widely used models of fringing capacitance are employed. The device is simulated with the help of commercially available finite element (FE) package PZFLEX. As experimental results for the entire range of values cannot be achieved, the FE results are regarded as closest to reality. The fractional percentage errors with respect to the simulated outcomes for the above three models are extracted. It is quite evident the fringing fields do exist in the CMUT structure and their inclusion in effectively modelling the CMUT is necessary.

2. Analytical model: The CMUT structure comprises of two parallel electrodes: one of Si_3N_4 membrane and the other of aluminium as shown in Fig. 2. The membrane is of t_m thickness, having a radius of value a_m. As the membrane is movable, a parallel-plate capacitor with variable separation is the standard equivalent used in the literature to demonstrate the effect of the transducer's geometry (electrode area and electrode separation) on the CMUT performance. The theoretical equation for the parallel-plate capacitor for gap separation t_g not comparable with the dimensions of the electrodes is, $C_g = \left(\varepsilon_g A\right)/t_g$, where A represents the area of the electrodes and ε_g is the permittivity of gap and is equal to 8.85×10^{-12} C^2/(N m^2), suggests a simple $1/x$ curvature for the plot of the measured capacitance versus separation distance.

Moreover, the thickness of the Si_3N_4 electrode is comparable with the gap separation between the plates; hence an equivalent capacitance C_{eff} is defined. C_{eff} of the device is the series capacitance of the membrane and the air gap capacitance without fringing effect, C_m and C_g, respectively. Accordingly, it is given by $1/C_{eff} = 1/C_m + 1/C_g$, which results in an effective distance d_{eff} and permittivity ε_{eff} for the device capacitance

$$\frac{d_{eff}}{\left(A\varepsilon_{eff}\right)} = \frac{t_m}{\left(A\varepsilon_m\right)} + \frac{t_g}{\left(A\varepsilon_g\right)} \tag{1}$$

It is assumed that the displacement of the membrane is small compared with the gap thickness. ε_m is the permittivity of Si_3N_4.

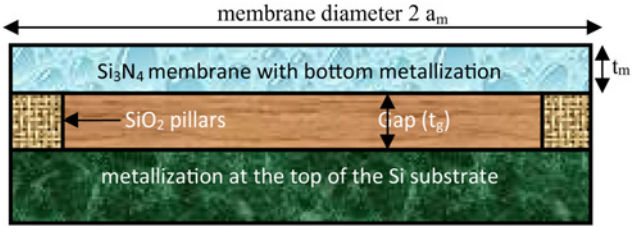

Fig. 2 *2D schematic diagram of an unbiased circular CMUT element*

Here, the membrane is assumed to be fully metallised. Pressure is defined as the force $F = -\left(dU/dt_g\right)$ per unit area as the gap separation varies with the applied bias. U is the potential energy and is equal to $\left(1/2\right)C_{eff}V(t)^2$, where $V(t)$ is the voltage applied across the CMUT. Now the force F is

$$F = -\left(\frac{dU}{dt_g}\right) = -\left(\frac{1}{2}\right) \times \frac{V(t)^2 C_m^2}{\left[\left(C_m/C_g\right)+1\right]^2 C_g^2} \times \frac{dC_g}{dt_g} \tag{2}$$

So, the membrane displacement at the centre of the structure w [13] at a membrane tension of T_m for modelling the CMUT will be given by

$$w = \left(\frac{1}{4AT_m}\right) \times \left(\frac{1}{2}\right) \frac{V(t)^2 C_m^2}{\left[\left(C_m/C_g\right)+1\right]^2 C_g^2} \times \left(\frac{\varepsilon_g A}{t_g^2}\right) \times a_m^2 \tag{3}$$

However, as the separation distance decreases, the simulated displacement starts to deviate from the theoretical value. This deviation becomes high as the gap size approaches the dimensions of the electrodes. Obviously, this deviation is due to the fringing field effect between the edges of the electrodes. There are several complicated approaches for including the fringing capacitance effect. One is the Palmer method for computing the fringing capacitance of a rectangular parallel-plate capacitor. This formulated is modified for application of CMUT [14]. The capacitance of the membrane C_{mf} inclusive of the excess electric fields at its ends for the Palmer method can be accounted as:

$$C_{mf} = \frac{\varepsilon_m A}{t_m}\left[1 + \frac{2t_m}{\pi^2 a_m} + \frac{2t_m}{\pi^2 a_m}\ln\left(\frac{\pi^2 a_m}{t_m}\right)\right] \times \left[1 + \frac{t_m}{2\pi a_m} + \frac{t_m}{2\pi a_m}\ln\left(\frac{4\pi a_m}{t_m}\right)\right] \tag{4}$$

Another simpler formula to account for the fringing effect of a circular disk parallel-plate capacitor is Landau and Lifschitz approach [15]. The excess fringing capacitance of the gap due to the excess electric fields at the ends of the electrodes can be accounted as $\varepsilon_g\left[a_m \ln\left\{\left(\left(16\pi a_m\right)/t_g\right)-1\right\}\right]$. The total capacitance of gap C'_{gf} and the membrane C'_{mf} is as follows:

$$C'_{gf} = \varepsilon_g\left[\left(\frac{\pi a_m^2}{t_g}\right) + a_m \ln\left\{\left(\frac{16\pi a_m}{t_g}\right)-1\right\}\right]$$
$$C'_{mf} = \varepsilon_m\left[\left(\frac{\pi a_m^2}{t_m}\right) + a_m \ln\left\{\left(\frac{16\pi a_m}{t_m}\right)-1\right\}\right] \tag{5}$$

The force on the membrane due to the applied bias V_{dc} can be written as

$$F = \frac{V_{dc}^2 C_{mf}'^2}{2\left\{\left(C'_{mf}/C'_{gf}\right)-1\right\}^2 C'^2_{gf}}\left[\frac{\varepsilon_g \pi a_m^2}{t_g^2} + \frac{16\pi a_m}{t_g^2}\left\{\frac{\varepsilon_g a_m}{\left(16\pi a_m/t_g\right)-1}\right\}\right] \tag{6}$$

Although this equation improves the calculated capacitance, it is far from being even close to the simulated value. An empirical approach, the Younes Ataiiyan's method [10], as presented in their technical report is used to equate the simulated membrane displacement to its theoretical value by replacing A, the membrane area, with $A_{effective}$, the effective area of the membrane in the form of $A_{effective} = A\left(74.5t_m + 0.82\right)$. This is similar to the correction being used for the length of a tube in the standing wave experiments

with sound. This equation reduces the difference between the simulated and calculated membrane displacements. Now, the capacitance of membrane C''_{mf} and the gap C''_{gf} is evaluated as follows:

$$C''_{mf} = \varepsilon_m\left[\frac{A_m(74.5t_m + 0.82)}{t_m}\right]$$
$$C''_{gf} = \varepsilon_g\left[\frac{A_m(74.5t_g + 0.82)}{t_g}\right] \quad (7)$$

As the capacitances of membrane and of the gap are connected in series, their equivalent capacitance C_{eq} will be given by $C_{eq} = \left[\left(C''_{mf} \times C''_{gf}\right)/\left(C''_{mf} + C''_{gf}\right)\right]$. Differentiating the gap capacitance with respect to electrode separation, we have $dC''_{gf}/dt_g = -\left[\left\{0.82\left(\varepsilon_g A\right)\right\}/t_g^2\right]$. So, the membrane displacement for Younes Ataiiyan's method for modelling the fringing field effect in CMUT will be given by

$$w = \left(\frac{1}{4AT_m}\right) \times \frac{1}{2} \times \frac{V_{dc}^2 C''^2_{mf}}{\left\{\left(C''_{mf}/C''_{gf}\right) + 1\right\}^2 C''^2_{gf}} \times \left(\frac{0.82\varepsilon_g A}{t_g^2}\right) \times a_m^2 \quad (8)$$

3. FE method (FEM) model: Modelling the CMUT with simulations uses the FEM analysis of the device. The displacement method associated with FEM is used for the analysis of CMUT behaviour. The structural geometry of the device is described in the coordinate axis. The structure is symmetric with respect to the *Y*-axis, and hence symmetric boundary conditions are applied on this axis. The structure is then broken into small interconnected elements which consist of a series of nodes. The process of arriving at the number of elements required is termed as meshing. A meshed CMUT circular membrane structure is shown in Fig. 3. The grid size is governed by the number of elements per wavelength. Assigning material properties is the most important step for all FEM models. The different structural materials are shown in Fig. 4 and their physical properties are listed in Table 1.

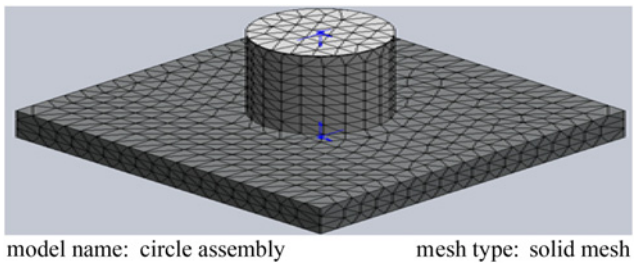

Fig. 3 *Gridded meshed structure of circular membrane CMUT*

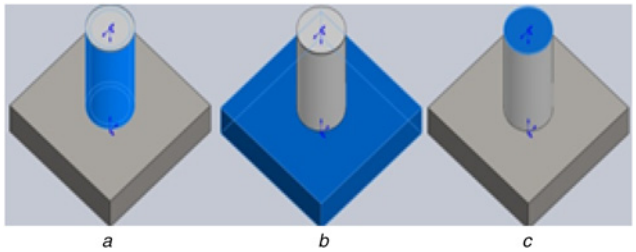

Fig. 4 *Different structural materials*
a SiO_2 pillars
b Si substrate
c Si_3N_4 membrane

Table 1 Physical properties of the structural materials used

Material name	SiO_2	Si	Si_3N_4
type	L, E, I	L, E, I	L, E, I
elastic modulus, GPa	310	169	320
Poisson's ratio	0.19	0.3	0.263
mass density, kg/m^3	2650	2330	3270

L: linear, E: elastic and I: isotropic.

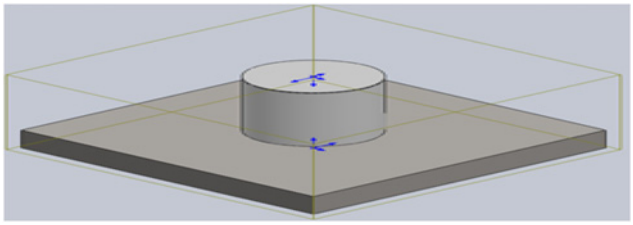

Fig. 5 *CMUT cell with global contact of air*

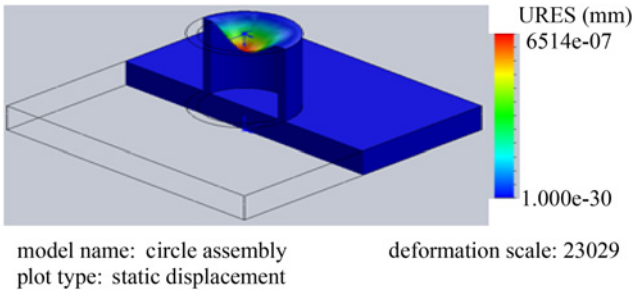

Fig. 6 *Displacement profile of the membrane*

Fig. 4 *a*, *b* and *c* respectively depict the SiO_2 pillars, Si substrate and Si_3N_4 membrane. The software computes the partial differential equations in each of the geometric division of the object, which is the FE. Adaptive meshing technique is utilised to build the model.

This ensures high accuracy in analysing the micromotion of the Si_3N_4 membrane with minimal calculation time. Optimised runtime is obtained by reducing the model mesh and inserting a loop into the model input file. Uniform pressure is applied on the surface of the Si_3N_4 membrane with air medium as the global contact as in Fig. 5. The deformed membrane with maximum displacement at the centre is shown in Fig. 6.

The work intents for an improved FEM which helps in predicting the transducer behaviour and can be improved in a simulation environment to accommodate the conditions required for a target of application such as medical imaging, non-destructive evaluation, chemical gas sensors and other applications. The fringing capacitance model predictions are in good agreement with the FEM results.

4. Results and discussion: The MUT device is simulated in the PZFLEX environment. As the device is symmetrical along the *Y*-axis, only half section of the structure is modelled, which greatly reduces the simulation time. The full structure of the device can be viewed by mirroring the axisymmetric model. The electrodes are considered to be infinitely thin and the bias and signal are applied at the lower layer of the upper electrode, which is the metallised Si_3N_4 layer. The variation of membrane displacement due to applied bias across the CMUT, membrane thickness, gap thickness and membrane radius is calculated using MATLAB. The parameter values used for theoretical calculations

doi: 10.1049/mnl.2017.0688

Table 2 Physical properties of the structural materials

Material properties	Value
gap thickness (t_g), μm	0.50
membrane radius (a_m), μm	25
silicon substrate thickness (t_s), μm	1
membrane thickness (t_m), μm	0.75
permittivity of the gap (ε_g), F/m	8.854×10^{-12}
density of the membrane (ρ_m), kg m^{-3}	3270
permittivity of the membrane (ε_m), F/m	4.1×10^{-11}
|DC dias (V_{dc}), V	40

are referred to Table 2. On the basis of these parameter values, the membrane displacement is calculated for the three approaches. For membrane displacement behaviour with respect to other parameters except bias, the bias is taken to be 40 V much below the collapse voltage region of operation of CMUT. At fixed bias of 40 V, the effect of other features, namely membrane thickness, gap separation and membrane radius is illustrated.

The CMUT is driven with a voltage $V(t) = V_{dc} + V_{ac} \cos \omega t$ that includes both bias and RF signal components. The square of this signal has a second harmonic content $V_{ac}^2 \cos^2 \omega t$. For operation at the first harmonic, the transducer is excited with signal amplitude V_{ac} much lower than the bias voltage V_{dc}. By making the bias voltage much larger than the time-varying voltage, the dominant force responsible for the membrane stretching becomes proportional to V_{dc}^2. Fig. 7 shows the variation of membrane displacement with the applied bias across the CMUT. w is directly proportional to V_{dc}^2, so there will be a parabolic opening up. As the applied bias across the membrane increases, then the force or pressure on membrane increases nonlinearly. The membrane displacement starts increasing from its initial zero displacement.

When the applied electrostatic potential increases then there will be a strong electrostatic force generated between the top and bottom electrodes and it will attract the top movable membrane toward the fixed substrate. As experimental results cannot be obtained for the entire region of operation, the FEM results are regarded as those closest to the reality. It is evident that the approaches with the fringing capacitance effect are more close to the simulated results than the model without fringing effect. The membrane displacement profiles for the three fringing capacitance evaluation methods are compared with simulation results and the modulus of the fractional % errors in membrane displacement are calculated.

Fig. 8 shows the fractional % of error values of the membrane centre displacement under a uniform pressure excitation across the CMUT. The empirical approach of Younes Ataiiyan shows a slope of error variation, which is opposite to the other two approaches. The average fractional % for the Younes Ataiiyan's approach for the entire region of bias voltage application below the collapse voltage is only 7%. For bias value below 80 V, which is quite high for generating the amplitude of the wave for use in medical imaging, the error is below 5%. This method models the membrane displacement quite effectively for variation in bias voltage. Moreover, at 40 V which is used in the experimental verification [16], the % error for above method is only 0.3%. Further investigation is done in the CMUT region of operation, where the displacement is enough to be used in medical imaging application as to which model best fits the CMUT behaviour.

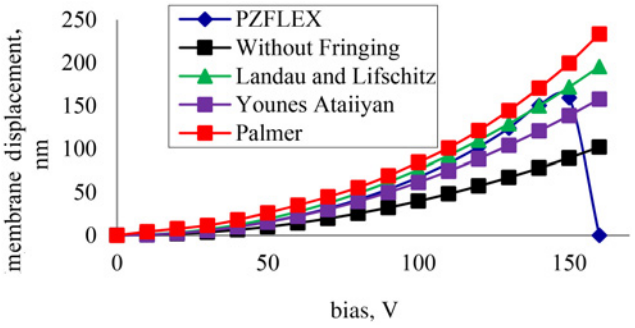

Fig. 7 *Membrane displacement behaviour with bias*

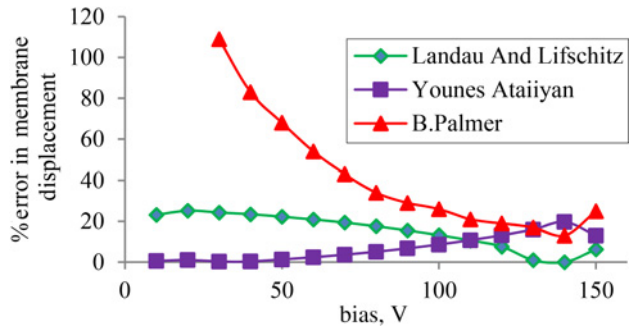

Fig. 8 *% Error in membrane displacement with respect to bias*

Figs. 9–14 show the membrane displacement profile and the fractional % of error values of the membrane centre displacement as a function of each critical parameter, the membrane radius, its thickness and the silicon dioxide (SiO_2) pillar height under a uniform pressure excitation. In each figure, all parameters except the one of interest are held constant. The significance of these figures is that they demonstrate how a CMUT membrane's displacement can be optimised with a change in structural geometries, which is a necessary condition for obtaining the required sensitivity. Fig. 9 shows the membrane centre displacement profile under a uniform pressure excitation across the CMUT for variation in membrane thickness and Fig. 10 shows the corresponding fractional percentage error. w is inversely proportional to t_m. As the membrane thickness increases at same bias and physical conditions, the flexibility of membrane decreases which decreases the electrostatic force of attraction between the membrane and substrate due to increase in

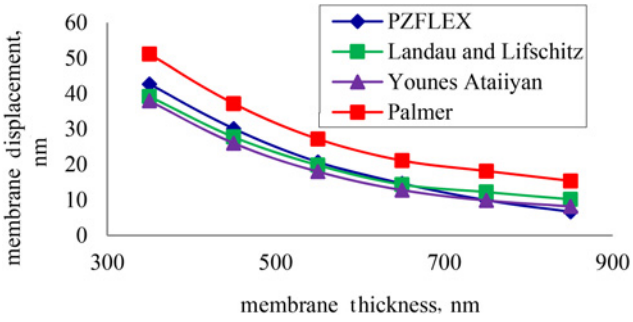

Fig. 9 *Membrane displacement with variation in membrane thickness*

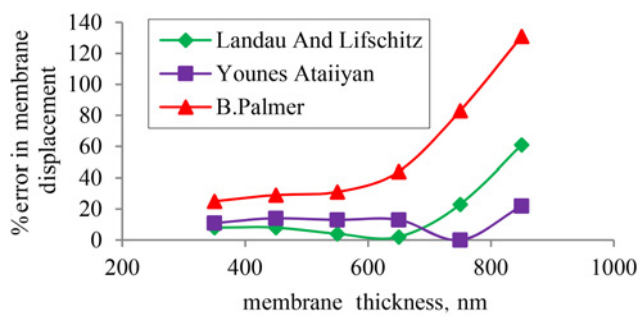

Fig. 10 *% Error in membrane displacement with membrane thickness*

stiffness of membrane. As a result, the displacement of the membrane decreases with increase in membrane thickness. Both the Landau and Ataiiyan approaches including the fringing effect show a close resemblance to the simulated outcome, more particularly the latter one, having a % of error nearly zero at a membrane thickness of 750 nm, which is used in the fabrication of CMUT [16].

Fig. 11 shows the membrane centre displacement profile under a uniform pressure excitation across the CMUT for variation in pillar height and Fig. 12 shows the corresponding % error variation. The electrostatic force of attraction is always dependent in inverse to the electrode separation. When the electrode space starts increasing, the coulombic force of attraction between the top and bottom electrodes starts decreasing. Hence the membrane displacement decreases. The electrode separation is made to vary between 50 nm and 0.5 μm as per with the present IC fabrication technology [17, 18]. The Younes Ataiiyan approach has very close resemblance to the simulated results.

Figs. 13 and 14 show the displacement profile and the % error in membrane displacement with variation in membrane radius, respectively. w is proportional to a_m^2, there will be a parabolic opening up. Tension is inversely related to length of string. With increase in the radius of the membrane, the tension (residual force) inside the membrane decreases. When the tension gets reduced, the membrane displacement due to same applied static bias will start increasing. Thus, displacement of membrane increases when the radius of circular membrane increases. Moreover, it is observed that at radius below 25 μm and also at larger membrane radii, the FEM output deviates from its usual characteristic as in the region from 25 to 40 μm radii. Such behaviour indicates that at these regions less energy is coupled to the surrounding medium, most of them are coupled to the substrate giving rise to Lamb and surface acoustic waves (SAWs), utilised extensively for sensor applications. Experiments have shown that an unavoidable side effect in the CMUT is the leakage of some energy into the substrate on which the device is built [19]. This coupling between the membrane and the substrate occurs through the membrane supports. Radiation pattern measurements in liquid media clearly identify this energy as that of a Lamb wave. At an operating frequency ~1 MHz, a Lamb wave device can be created by exploiting this phenomenon such that the CMUT is optimised to couple energy into the substrate.

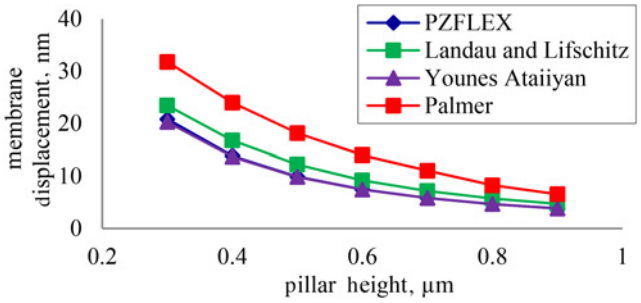

Fig. 11 *Membrane displacement with variation in gap thickness*

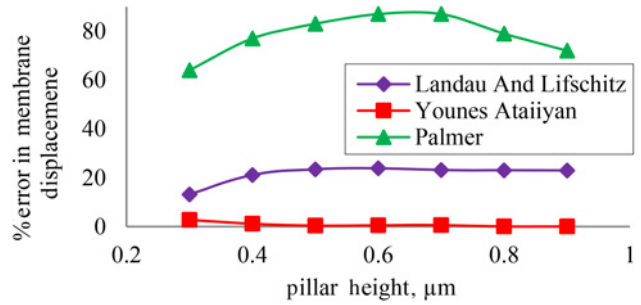

Fig. 12 *% Error in membrane displacement with a height of the pillar*

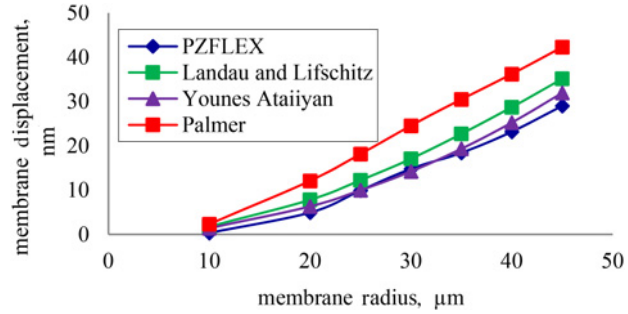

Fig. 13 *Membrane displacement with variation in membrane radius*

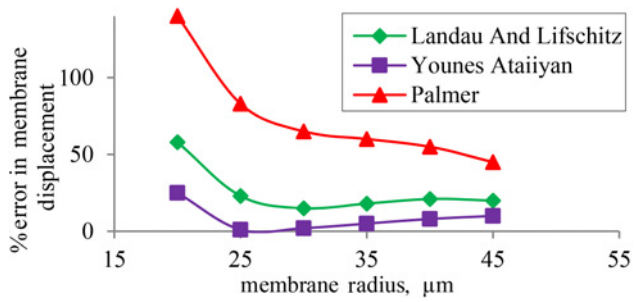

Fig. 14 *% Error in membrane displacement with membrane radius*

At higher frequencies, beyond 40 μm of membrane radius, it is the leaky SAWs that dominate. Hence, the other parameters being unchanged membrane radii of 25–40 μm are best suited for medical imaging purposes. In this region, the Ataiiyan's model follows the PZFLEX output. At radius values <10 μm, the membrane becomes too rigid to produce vibrations as in Fig. 12. Above 50 μm radius, the frequency of vibration is far below the medical imaging regime. A comparative analysis of the average % errors for the modelling approaches is shown in Table 3.

The FEM model not only predicts the first resonant frequency but the higher-resonant frequencies corresponding to the higher-bending modes of the diaphragm [20] are also evaluated as

Table 3 Comparative analysis of the % errors with critical parameters

Critical parameters				Palmer	Landau and Lifschitz	Younes Ataiiyan
Bias, V	t_m, nm	a_m, μm	t_g, nm			
—	750	26	500	41.62	15.61	7.14
40	—	26	500	57.17	17.67	12.17
40	750	26	—	78.17	21.29	0.57
40	750	—	500	76.5	27	13.66

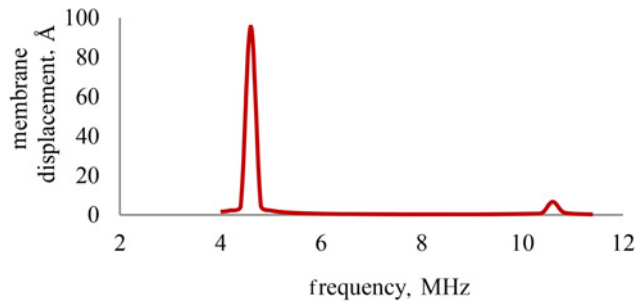

Fig. 15 *Frequency response of CMUT cell*

doi: 10.1049/mnl.2017.0688

shown in Fig. 15. The fundamental resonant frequency evaluated is 4.58 MHz while that shown by Ayhan *et al.* is 4.5 MHz [16].

5. Conclusion: The capacitances of membrane and gap are determined using the Palmer's, Landau's and Younes Ataiiyan's method. Using Mason's modelling of circular membrane approximation, the membrane displacement is calculated. The effect of applied bias across the CMUT, membrane thickness, gap separation and membrane radius on membrane displacement is determined. These membrane displacement profiles are compared with the FEM results, and the % error in membrane displacement corresponding to each parameter is determined. The result shows that the Younes Ataiiyan's method for modelling the fringing field effect in CMUT is closest to the simulation result. The membrane displacement profile bias variation is approximately same as simulation result up to 80 V but from thereafter it deviates somewhat having an average error for the entire region of applied bias of only 7%. The membrane displacement profile for gap separation is approximately same as a simulation result. However, other membrane displacement profiles deviate somewhat. So, there is a scope for further improvement using other methods to minimise the % error in membrane displacement corresponding to each parameter.

6. Acknowledgment: The authors are highly indebted to the University Grant Commission, Ministry of Human Research Development (MHRD), Government of India for supporting this technical work.

7 References

[1] Chen K., Lee H., Sodini C.: 'A column-row-parallel ASIC architecture for 3-D portable medical ultrasonic imaging', *IEEE J. Solid-State Circuits*, 2016, **51**, (3), pp. 738–752

[2] Boulmé A., Ngo S., Minonzio J., *ET AL.*: A capacitive micromachined ultrasonic transducer probe for assessment of cortical bone', *IEEE Trans. Ultrason. Ferroelectr. Freq. Control*, 2014, **61**, (4), pp. 710–723

[3] Gurun G., Tekes C., Zahorian J., *ET AL.*: 'Single-chip CMUT-on-CMOS front-end system for real-time volumetric IVUS and ICE imaging', *IEEE Trans. Ultrason. Ferroelectr. Freq. Control*, 2014, **61**, (2), pp. 239–250

[4] Savoia A., Caliano G., Pappalardo M.: 'A CMUT probe for medical ultrasonography: from microfabrication to system integration', *IEEE Trans. Ultrason. Ferroelectr. Freq. Control*, 2012, **59**, (6), pp. 1127–1138

[5] Cheng T., Tsai T.: 'CMOS ultrasonic receiver with on-chip analog-to-digital front end for high-resolution ultrasound imaging systems', *IEEE Sens. J.*, 2016, **16**, (20), pp. 7454–7463

[6] Miao J., Wang H., Li P., *ET AL.*: 'Glass-SOI-based hybrid-bonded capacitive micromachined ultrasonic transducer with hermetic cavities for immersion applications', *J. Microelectromech. Syst.*, 2016, **25**, (5), pp. 976–986

[7] Kumar M.J., Gupta S., Venkataraman V.: 'Compact modelling of the effects of parasitic internal fringe capacitance on the threshold voltage on high-k gate-dielectric nano scale SOI MOSFETs', *IEEE Trans. Electron. Devices*, 2006, **53**, (4), pp. 706–711

[8] Vitaly L., David E.: 'Fringing field effect in electrostatics actuators'. Technical Report ETR-2004-2, Israel Institute of Technology, Israel, 2004

[9] Hosseini M., Zhu G., Peter Y.: 'A new formulation of fringing capacitance and its application to the control of parallel-plate electrostatic micro actuators', *Analog Integr. Circuit Signal Process.*, 2007, **53**, (3), pp. 119–128

[10] Burt S., Finney N., Young J.: 'Fringing field of parallel plate capacitor'. Available at http://www.santarosa.edu, accessed 14th September 2017

[11] Guha K., Kumar M., Aggarwal S., *ET AL.*: 'Modified capacitance model of RF MEMS shunt switching incorporating fringing field effects of perforated beam', *Solid State Electron.*, 2015, **114**, pp. 35–42

[12] Rahman M., Hernandez J., Chowdhury S.: 'An improved analytical method to design CMUTs with square diaphragms', *IEEE Trans. Ultrason. Ferroelectr. Freq. Control*, 2013, **60**, (4), pp. 834–844

[13] Maity R., Maity N., Baishya S.: 'Circular membrane approximation model with the effect of the finiteness of the electrode's diameter of MEMS capacitive micromachined ultrasonic transducers', *Microsyst. Technol.*, 2017, **23**, (8), pp. 3513–3524

[14] Palmer B.: Capacitance of a parallel-plate capacitor by the Schwartz–Christoffel transformation', *Trans. Am. Inst. Electr. Eng. (AIEE)*, 1937, **56**, (5), pp. 363–366

[15] Landau L., Lifschitz E.: 'Electrodynamics of continuous media' (Permagon Press, Oxford, England, 1987)

[16] Bozkurt A., Igal Ladabaum I., Khuri-Yakub B.T.: 'Theory and analysis of electrode size optimization for capacitive microfabricated ultrasonic transducers', *IEEE Trans. Ultrason. Ferroelectr. Freq. Control*, 1999, **46**, (6), pp. 1364–1374

[17] Buhrdorf A., Ahrens O., Binder J.: 'Capacitive micromachined ultrasonic transducers and their application', *IEEE Ultrason. Symp.*, 2001, pp. 933–940

[18] Tsuji Y., Kupnik M., Khuri-Yakub B.T.: 'Low temperature process for CMUT fabrication with wafer bonding technique', *IEEE Ultrason. Symp.*, 2010, pp. 551–554

[19] Yaralioglu G., Degertekint F., Badi M., *ET AL.*: 'Finite element method and normal mode modeling of capacitive micromachined saw and lamb wave transducers', *IEEE Ultrason. Symp.*, 2000, pp. 129–132

[20] Caronti A., Majjad H., Ballandras S., *ET AL.*: 'Vibration maps of capacitive micromachined ultrasonic transducers by laser interferometry', *IEEE Trans. Ultrason. Ferroelectr. Freq. Control*, 2002, **49**, (3), pp. 289–292